nanomaterials

MDPI

Article

Sn-Doping and Li_2SnO_3 Nano-Coating Layer Co-Modified $LiNi_{0.5}Co_{0.2}Mn_{0.3}O_2$ with Improved Cycle Stability at 4.6 V Cut-off Voltage

Huali Zhu [1], Rui Shen [1], Yiwei Tang [2], Xiaoyan Yan [3], Jun Liu [3], Liubin Song [4], Zhiqiang Fan [1], Shilin Zheng [2] and Zhaoyong Chen [3,*]

1 School of Physics and Electronic Science, Changsha University of Science and Technology, Changsha 410114, China; juliezhu2005@126.com (H.Z.); 18271692161@163.com (R.S.); zqfan@csust.edu.cn (Z.F.)
2 Qinyuan Jiazhi Institute Co. Ltd., Qingyuan 511517, China; tangyiwei@jianae.com (Y.T.); zhengshilin@jianae.com (S.Z.)
3 School of Materials Science and Engineering, Changsha University of Science and Technology, Changsha 410114, China; richardhipower@126.com (X.Y.); liujun@stu.csust.edu.cn (J.L.)
4 School of Chemistry and Food Engineering, Changsha University of Science and Technology, Changsha 410114, China; liubinsong1981@126.com
* Correspondence: chenzhaoyong@csust.edu.cn; Tel.: +86-731-13787112902

Received: 11 April 2020; Accepted: 27 April 2020; Published: 30 April 2020

Abstract: Nickel-rich layered $LiNi_{1-x-y}Co_xMn_yO_2$ ($LiMO_2$) is widely investigated as a promising cathode material for advanced lithium-ion batteries used in electric vehicles, and a much higher energy density in higher cut-off voltage is emergent for long driving range. However, during extensive cycling when charged to higher voltage, the battery exhibits severe capacity fading and obvious structural collapse, which leads to poor cycle stability. Herein, Sn-doping and in situ formed Li_2SnO_3 nano-coating layer co-modified spherical-like $LiNi_{0.5}Co_{0.2}Mn_{0.3}O_2$ samples were successfully prepared using a facile molten salt method and demonstrated excellent cyclic properties and high-rate capabilities. The transition metal site was expected to be substituted by Sn in this study. The original crystal structures of the layered materials were influenced by Sn-doping. Sn not only entered into the crystal lattice of $LiNi_{0.5}Co_{0.2}Mn_{0.3}O_2$, but also formed Li^+-conductive Li_2SnO_3 on the surface. Sn-doping and Li_2SnO_3 coating layer co-modification are helpful to optimize the ratio of Ni^{2+} and Ni^{3+}, and to improve the conductivity of the cathode. The reversible capacity and rate capability of the cathode are improved by Sn-modification. The 3 mol% Sn-modified $LiNi_{0.5}Co_{0.2}Mn_{0.3}O_2$ sample maintained the reversible capacity of 146.8 mAh g^{-1} at 5C, corresponding to 75.8% of its low-rate capacity (0.1C, 193.7mAh g^{-1}) and kept the reversible capacity of 157.3 mAh g^{-1} with 88.4% capacity retention after 100 charge and discharge cycles at 1C rate between 2.7 and 4.6 V, showing the improved electrochemical property.

Keywords: lithium-ion batteries; cathode material; $LiNi_{0.5}Co_{0.2}Mn_{0.3}O_2$; Sn-modification; high cut-off voltage

1. Introduction

The lithium-ion battery (LIB) is one of the most promising power supply devices for portable electronic products and electric vehicles because of its high energy density and power density, long cycle lifetime and environmental benignity among various novel battery systems [1–5]. Because the commercialized $LiCoO_2$ cathode material has the disadvantages of high cost and poor thermal safety, the aim of present research work is to develop the prospective alternatives for $LiCoO_2$ toward

better lithium batteries [6–10]. Nickel-rich layered $LiMO_2$ is an important cathode material for LIB because of its superior theoretical discharge capacity compared with that of olivine or spinel materials. Herein, high nickel content in $LiMO_2$ is beneficial to increase capacity, high manganese content enhances the structural stability and high cobalt content improves the rate performance [11]. Among these $LiMO_2$ materials, $LiNi_{0.5}Co_{0.2}Mn_{0.3}O_2$ has been gradually used as a component of commercial lithium secondary batteries due to its low price, high capacity and improved safety. Nevertheless, $LiNi_{0.5}Co_{0.2}Mn_{0.3}O_2$ still suffers from several issues, including severe capacity degradation and limited high-rate capability, especially at high cut-off voltage, which is ascribed to the transition metal dissolution and surface structure transformation during cycling [11].

At present, surface coating has been implemented to improve the cyclic property of cathode materials. Coatings like metal oxides (such as Al_2O_3 [12,13], antimony doped tin oxide (ATO) [14], CeO_2 [15], CuO [16], Cr_8O_{21} [17], MoO_3 [18], SiO_2 [19], TiO_2 [20], ZnO [21], and ZrO_2 [22]), fluoride (AlF_3 [23]), lithium salts (such as $LiAlO_2$ [24], $LiBO_2$ [25], Li_2MnO_3 [26], Li_2MoO_4 [27], Li_2SiO_3 [28], Li_2TiO_3 [29], Li_3VO_4 [30], and Li_2ZrO_3 [31]), and others (polypyrrole (PPy) [32], carbon nanotube (CNT) [33]) are proven to be effective for alleviating the transition metal dissolution and then improving the cyclic property of the cathode materials. On the other side, partial substitution with cations or anions is considered as a promising method to stabilize the crystalline structure of $LiNi_{0.5}Co_{0.2}Mn_{0.3}O_2$ materials and improve its high-rate capability, such as bulk doping with Al [24,34,35], K [36], Mo [37], Na [38,39], Nd [40], Ti [41,42], Zr [22,32,42], Y [43], F [44], and Cl [36]. In principle, researchers choose the ions which show a large ionic radius and high electronegativity to substitute for the transition metals in $LiMO_2$ because these kinds of ions can expand the channel-like Li^+ diffusion pathway and decrease the covalence characteristics of cation–oxygen bonds of $LiMO_2$ materials. Ion substitution inhibits the release of oxygen and has little effect on the structure of $LiNi_{0.5}Co_{0.2}Mn_{0.3}O_2$ materials, so the host lattice of the materials will be well maintained. As we know, the electrochemical properties of $LiMO_2$ materials can be greatly enhanced when combined with the advantages of doping and coating co-modification by $LiAlO_2$-coating layer and Al-dopant [24]. Mo-coating and doping for $LiNi_{0.5}Co_{0.2}Mn_{0.3}O_2$ [45] have been studied by researchers and demonstrated enhanced electrochemical properties.

Among various doping cations, Sn^{4+} has the same ionic radius of 0.69 Å as Ni^{2+}, close to that of Li^+ (0.76 Å). Meanwhile, the bonding energy of Sn-O is 548 kJ mol^{-1}, while those of Ni-O, Co-O and Mn-O are 391.6, 368 and 402 kJ mol^{-1}, respectively. The high bonding energy of Sn-O is favorable to improve the crystalline structural stability of cathode materials. In addition, Sn^{4+} has a high electronegativity, leading to strong ionicity of the metal–oxygen bond [46]. Therefore, Sn-modification is expected to enhance the cyclic property and high-rate capability of $LiMO_2$ materials. The rate performances of some layered $LiMO_2$ materials have been enhanced by substituting stannum for transition metals. For example, $LiNi_{3/8}Co_{2/8}/Mn_{3/8-x}Sn_xO_2$ has enhanced the chemical diffusion coefficient D_{Li} of Li-ion, leading to improved rate capability [47]. Sn-doped $LiNi_{0.8}Co_{0.2}O_2$ has increased electronic conductivity because a free electron was released into the conduction band after doping [48]. The electrochemical properties of $LiNi_{0.8}Co_{0.1}Mn_{0.1}O_2$ have been enhanced by SnO_2 at high voltage [49].

In this study, we report a facile synthesis of Sn-doping and Li_2SnO_3 in situ coating layer co-modified (Sn-modified) $LiNi_{0.5}Co_{0.2}Mn_{0.3}O_2$. The crystalline structures, morphologies, surface chemical states of cations and electrochemical performances of Sn-modified $LiNi_{0.5}Co_{0.2}Mn_{0.3}O_2$ samples are characterized. As expected, the amount of Sn has a major impact on the modification treatment. Substituting a large amount of Sn for transition metals in $LiNi_{0.5}Co_{0.2}Mn_{0.3}O_2$ can form Li_2SnO_3 on the surface. Suitable Sn-substituting can relieve the cation mixing degree and provide a stable structure as well as form the Li^+-conductive coating layer on the surface of the sample, leading to improved physical and electrochemical properties.

2. Materials and Methods

2.1. Materials Preparation

Layered Sn-modified $LiNi_{0.5}Co_{0.2}Mn_{0.3}O_2$ samples were synthesized using a facile molten salt method. Molten salt ($0.76LiOH{\cdot}H_2O$–$0.12Li_2CO_3$), commercial $Ni_{0.5}Co_{0.2}Mn_{0.3}(OH)_2$ precursors and nano-sized Sn powder were used as raw materials and mixed completely by mortar and pestle with the appropriate amount of ethyl alcohol. $LiOH{\cdot}H_2O$ with a purity of 98% was bought from Xilong Chemical Co., Ltd. (Shantou, China). Li_2CO_3 with a purity of 99.5% was provided by Sichuan Tianqi Lithium Co., Ltd (Chengdu, China). $Ni_{0.5}Co_{0.2}Mn_{0.3}(OH)_2$ with a transition metal element content of 62.27% was purchased from Chongqing Teri battery materials Co., Ltd. (Chongqing, China). Sn powder with a purity of 99.9% was bought from Shanghai Chaowei Nano Technology Co., Ltd. The molar ratio of the Li and M in $LiMO_2$ was 1.05:1. The mixture was pre-heated at 480 °C for 120 min followed by calcination at 880 °C for 720 min in air atmosphere. Finally, the obtained samples were ground for 30 min for physical and electrochemical property tests. Here, Sn-modified $LiNi_{0.5}Co_{0.2}Mn_{0.3}O_2$ compounds, in which certain amounts of transition metals were substituted by Sn, were marked as MS1 (1 mol% Sn), MS3 (3 mol% Sn) and MS5 (5 mol% Sn), and were prepared via the above-mentioned approaches. The pristine $LiNi_{0.5}Co_{0.2}Mn_{0.3}O_2$ compounds were obtained through the same method and labeled as M523.

2.2. Characterizations

The crystalline structures of synthesized $LiNi_{0.5}Co_{0.2}Mn_{0.3}O_2$ materials were characterized using X-ray diffraction (XRD, D/Max 2000/PC, Rigaku, Tokyo, Japan) with Cu Kα radiation (λ = 1.54056 Å) from 10° to 90° with a scan rate of 5° per min. The morphologies of modified samples were characterized by scanning electron microscopy (SEM, Sirion200, FEI Ltd., Eindhoven, The Netherlands). The microstructure of the sample surface was analyzed using transmission electron microscopy (TEM, TECNAI G2 F20, FEI Company, Hillsboro, USA). The element distributions were determined using energy dispersive X-ray spectroscopy (EDS, Model 7426, Oxford, UK). The surfaces of the samples were examined using X-ray photoelectron spectroscopy (XPS, K-Alpha 1063, Thermo Fisher Scientific, Waltham, MA, USA) with AlKα line (1486.6 eV) as the source of X-ray.

The CR2025 cell assembly process, the electrochemical charge and discharge tests and the electrochemical impedance spectroscopy (EIS) tests were conducted according to the experimental section of our recently published article [36].

3. Results and Discussion

The crystalline structures of the Sn-modified $LiNi_{0.5}Co_{0.2}Mn_{0.3}O_2$ samples were studied using XRD in order to characterize the effects of Sn-substitution on the crystal, and the typical diffraction patterns of all samples are demonstrated in Figure 1. The XRD patterns of well-crystallized pristine and Sn-modified $LiNi_{0.5}Co_{0.2}Mn_{0.3}O_2$ samples were all indexed to a hexagonal α-$NaFeO_2$ layered structure (*R*-3*m* space group) with sharp and clear diffraction peaks. The obvious splitting of diffraction peaks of (006)/(102) and (108)/(110) reflects the highly ordered hexagonal structure. However, there are some impurities in the patterns of samples MS3 and MS5 near the 2θ of 35 and 43°, which are identified as Li_2SnO_3. It is obvious that the formation of Li_2SnO_3 phase is related to the amount of dopant. To identify the effects of tin substitution on the structures of Sn-modified samples, the crystallographic data of samples are demonstrated in Table 1. Even though the doping amount was small, the cell parameters of all samples changed, showing that Sn-modification affected the main structure of the host. All the crystallographic data changed, which suggests that the substituting element entered into the crystal lattice. All the crystallographic data ratios c/a are higher than 4.899, showing the highly ordered crystal structure. The I_{003}/I_{104} ratios (*R*) of modified samples are larger than the value of 1.2, indicating that Sn-substituting can relieve the cation mixing degree. That is to say, Sn^{4+} helps to stabilize the crystal structure of $LiNi_{0.5}Co_{0.2}Mn_{0.3}O_2$ during the Li^+ intercalation and de-intercalation process

because Sn-O has a higher bonding energy than those of transition metals and oxygen. The 3 mol% substituting sample showed the largest intensity ratio $R'((I_{006}+ I_{102})/I_{101})$ and crystal volume, which may have resulted in the best electrochemical performance.

The SEM images of Sn-modified $LiNi_{0.5}Co_{0.2}Mn_{0.3}O_2$ samples and the EDS images are displayed in Figure 2. As is shown, there were no significant differences in the grain sizes from the pristine and Sn-modified samples. All the compounds showed a spherical-like morphology with a particle size from 4 to 6 μm, which is made up by lots of fine primary particles with a length range of 0.5–1 μm. The sample surface was not only compact but also provided enough surface area to make full contact between the cathode and the electrolyte. According to the EDS measurements showing in Figure 2k, it can be obviously seen that stannum and transition metals were uniformly distributed on the surface of the MS3 compound.

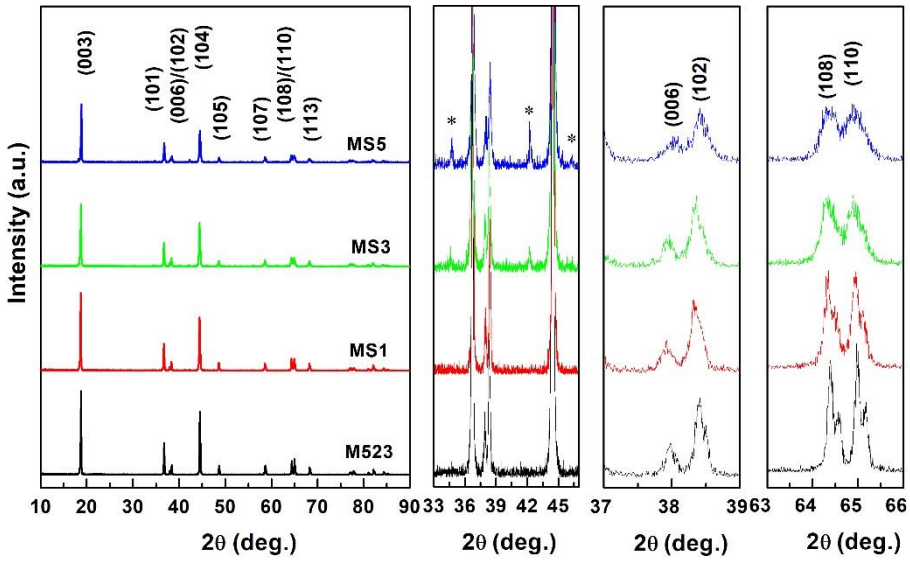

Figure 1. XRD patterns of Sn-modified $LiNi_{0.5}Co_{0.2}Mn_{0.3}O_2$ samples (∗ represents Li_2SnO_3).

Table 1. Lattice constants of Sn-modified $LiNi_{0.5}Co_{0.2}Mn_{0.3}O_2$ samples.

Sample	*a* (Å)	*c* (Å)	*c*/*a*	$R(I_{003}/I_{104})$	$R'((I_{006}+ I_{102})/I_{101})$	V (Å^3)
M523	2.8673	14.2103	4.956	1.319	0.428	101.18
MS1	2.8694	14.2286	4.959	1.460	0.474	101.46
MS3	2.8710	14.2223	4.954	1.425	0.526	101.53
MS5	2.8715	14.1499	4.928	1.821	0.508	101.04

To reveal the in situ formation of the Li_2SnO_3 on the surface of the samples, the microstructure of Sn-modified $LiNi_{0.5}Co_{0.2}Mn_{0.3}O_2$ sample MS3 was examined using TEM as shown in Figure 3. It can be seen from Figure 3a that a nano-sized coating layer was obtained on the particle surface of MS3. Three of the coating sites (Figure 3b–d) were enlarged in order to observe the thin layer more clearly. The surface coating layer, which uniformly adhered to the bulk of MS3 particles, had a thickness within the range of 5–10 nm. In addition, Figure 3b,c clearly indicates the crystalline interplanar spacing of 0.495 and 0.228 nm, which can be indexed as (002) and (–221) facets of Li_2SnO_3 (JCPDS no. 31-0761), respectively. The (003) facet of bulk MS3 with the crystalline interplanar spacing of 0.478 nm is demonstrated in Figure 3d. These results were consistent with the XRD result and further identified the formation of Li_2SnO_3 nano-coating layer.

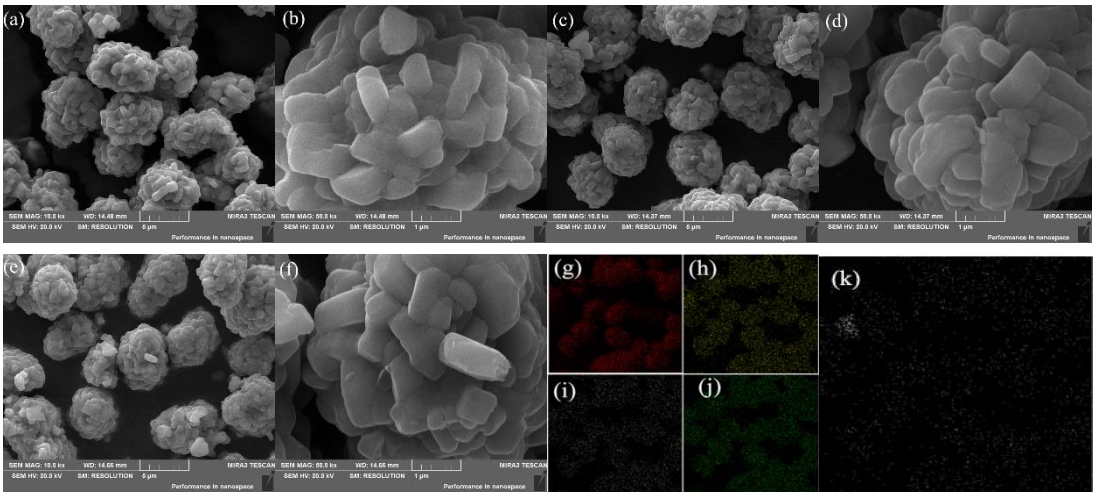

Figure 2. SEM images of MS1 (**a**,**b**), MS3 (**c**,**d**), MS5 (**e**,**f**), and the corresponding EDS mappings of image MS3 (**c**): (**g**)-O, (**h**)-Ni, (**i**)-Co, (**j**)-Mn, (**k**)-Sn.

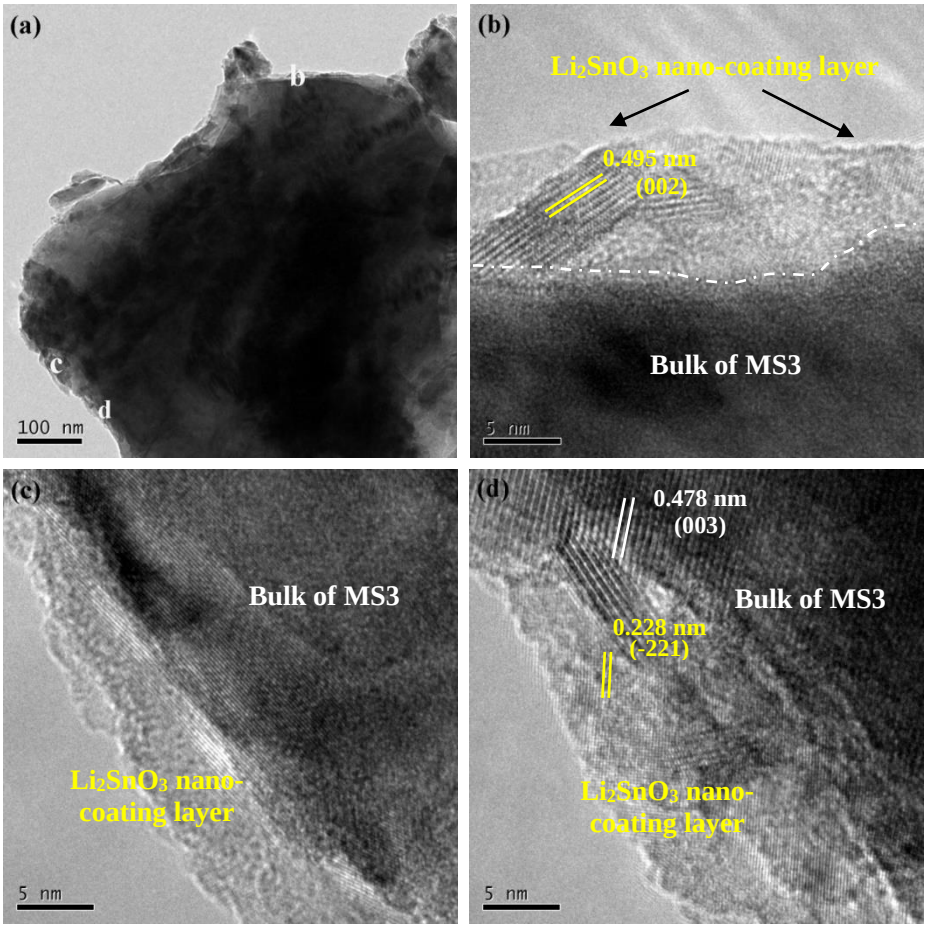

Figure 3. TEM images of MS3 (**a**) and the selected areas in Figure 3a (**b**–**d**).

To understand the surface chemical composition of the transition metal elements (Ni, Co, Mn) and Sn, the pristine M523 and Sn-modified sample MS3 were examined using XPS. The XPS patterns are shown in Figure 4 and Figure S1. Compared to the pristine M523, the peak positions of Co $2p_{3/2}$ and Mn $2p_{3/2}$ in 3 mol% Sn-modified sample MS3 had no obvious shift, showing that the surface chemical states of the transition metals did not change. To further clarify the effect of Sn-modification on the chemical states of cations, the peak positions and mole fractions of transition metal ions and

Sn^{4+} in the crystal of M523 and MS3 compounds deduced from XPS fittings are listed in Table 2. According to the corresponding binding energies of Ni $2p_{3/2}$, Co $2p_{3/2}$ and Mn $2p_{3/2}$, we can ascertain that the chemical valences of Ni are Ni^{2+} (853.6 and 854.7 eV) and Ni^{3+}(856.2 eV), while those of Co and Mn are Co^{3+} (779.8 eV) and Mn^{4+} (642.4 eV), respectively. The results show that the oxidation valences of Ni, Co and Mn in the Sn-modified samples are still the same as those of the pristine one, only that the mole fraction ratio of Ni^{2+}/Ni^{3+} increased from 72.27%/27.73% to 74.88%/25.12% after Sn-modification, which indicates that MS3 has better structure stability. Sn3d peaks appear at 486.5 and 494.9 eV, showing that Sn exists in +4 chemical state [47]. Additionally, Sn-modification has a great influence on the chemical state of O1s. The peak at 529.35 eV was caused by the interaction of transition metal ions and oxygen in the crystal structure, and the peak at 531.54 eV is related to formation of lithium carbonate at the sample surface [50]. The peak intensities of the two characteristic peaks of O1s occur in deflection, which indicates that the lattice oxygen increased and the adsorbed oxygen on the surface decreased after modification. It is beneficial to keep the layered structure stable and reduce the formation of impurities on the sample surface.

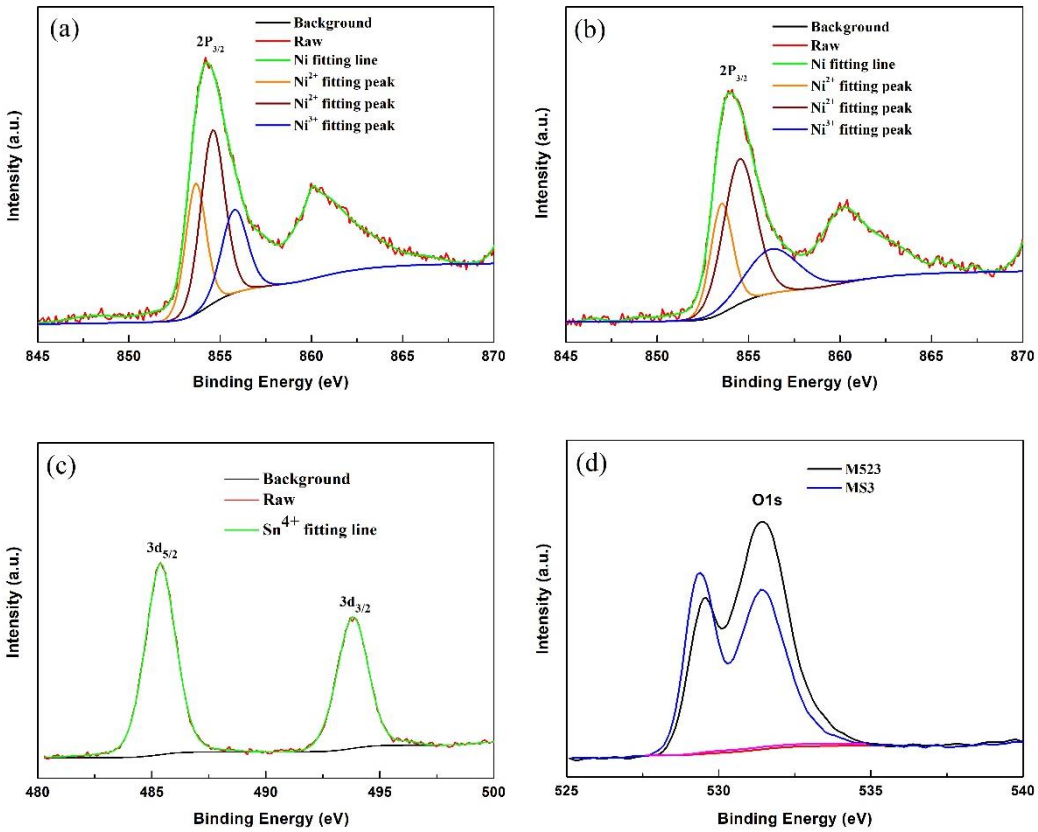

Figure 4. XPS spectra of the synthesized materials: Ni $2p_{3/2}$ (**a**) spectra of M523, Ni $2p_{3/2}$ (**b**), Sn3d (**c**) spectra of MS3, O1s (**d**) spectra of M523 and MS3.

Table 2. Peak positions and mole fractions of the metal elements for M523 and MS3 samples obtained from XPS fittings.

	Sample	Elements					
		Ni^{2+}		Ni^{3+}	Co^{3+}	Mn^{4+}	Sn^{4+}
Peak position/eV	M523	853.6	854.7	856.2	779.8	642.4	–
	MS3	853.6	854.7	856.2	779.8	642.4	486.4
Mole fraction/%	M523	72.27		27.73	100.0	100.0	–
	MS3	74.88		25.12	100.0	100.0	100.0

The curves of electrochemical performance are characterized in Figure 5. The initial charge and discharge capacities were tested at 0.1 C rate at room temperature. We can determine from Figure 5a that the initial discharge capacities for the M523, MS1, MS3 and MS5 samples are 203.9, 196.8, 193.7 and 188.0 mAh g^{-1}, and the corresponding coulombic efficiencies are 79.2%, 82.6%, 84.9% and 84.0%, respectively. As discussed previously, a large amount of Sn-doping and Li_2SnO_3 impurity existed in MS5, which probably led to the lowest initial discharge capacity. The coulombic efficiency values of the Sn-modified samples are all higher than that of the pristine one. This should be attributed to the Sn-substituting, which can relieve the cation mixing degree and is favorable for Li^+ transfer.

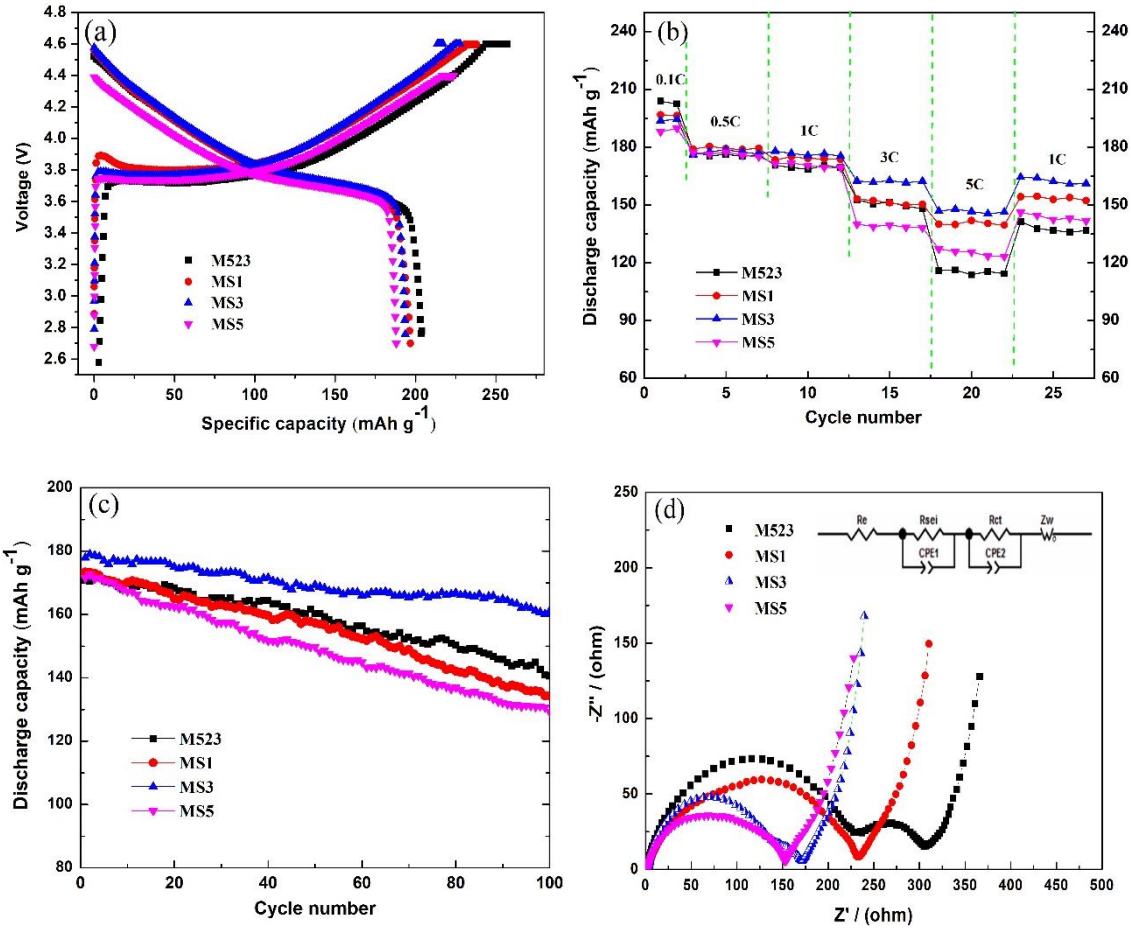

Figure 5. Electrochemical performance of Sn-modified $LiNi_{0.5}Co_{0.2}Mn_{0.3}O_2$ samples: (**a**) Initial charge–discharge curves at 0.1C, (**b**) rate performance from 0.1 to 5C, (**c**) cyclic ability at 1C, and (**d**) electrochemical impedance spectroscopy (EIS) plots of Sn-modified $LiNi_{0.5}Co_{0.2}Mn_{0.3}O_2$ samples after the 100th cycle.

The rate performances of $LiNi_{0.5}Co_{0.2}Mn_{0.3}O_2$ samples are compared in Figure 5b, in which the charge–discharge cycle was successively taken from 0.1 to 5 C at 2.7–4.6 V for every five cycles. The Sn-modified samples displayed more enhanced rate performance than the pristine M523 at high rates. The MS3 sample presented a reversible capacity of 146.8 mAh g^{-1} at 5 C, corresponding to 75.8% of its initial capacity (0.1C, 193.7mAh g^{-1}). However, the pristine M523 kept a reversible capacity of 116.0 mAh g^{-1}, just 56.9% of its initial capacity (0.1C, 203.9 mAh g^{-1}). This can be attributed to the fact that the bonding energy of Sn–O is higher than those of the transition metal and oxygen in $LiNi_{0.5}Co_{0.2}Mn_{0.3}O_2$ samples. It can be seen from the previous XRD results that Sn-substituting can relieve the cation mixing degree and benefit the Li^+ intercalation/de-intercalation, even in high current density. Furthermore, the formed Li^+-conductive Li_2SnO_3 nano-coating layer prevents the side reaction at the cathode and the electrolyte interface and accelerates the transport of lithium ions as well.

The cyclic stability properties of Sn-modified $LiNi_{0.5}Co_{0.2}Mn_{0.3}O_2$ at 1C are illustrated in Figure 5c. It is observed that the Sn-modified sample MS3 exhibited excellent capacity retention with a capacity of 157.3mAh g^{-1} and discharge capacity retention of 88.4% at the 100th cycle, while the pristine sample M523 only kept a capacity of 124.9 mAh g^{-1} and discharge capacity retention of 73.2%. These results indicate that Sn-modification is favorable for keeping the structural stability of the pristine materials and obtaining enhanced cycle performance. Doping can improve the conductivity of the material, and the increase of conductivity after a small amount of doping is reflected in the increase of capacity; however, with the increase of doping amount, the active material decreases, resulting in the loss of electrochemical capacity. Therefore, there is a lack of continuous changes for data shown in Figure 5b,c with the trend of MS5 < MS3 < MS1 or MS1 < MS3 < MS5.

To better understand the effect of Sn-modification on the electrochemical properties of cathode materials, EIS analysis was carried out. Figure 5d demonstrates the EIS profiles of the Sn-modified $LiNi_{0.5}Co_{0.2}Mn_{0.3}O_2$ cathodes after the 100th cycle at 1C. According to the equivalent circuit [40] in the inset in which R_{sei} stands for the resistance of solid electrolyte interface (SEI) layer, R_{ct} is the charge transfer impedance at the interface of electrolyte–electrode, and Z_w is the Li ion diffusion in the crystal lattice, the EIS spectra were analyzed using Zview-2 software. The values of the total resistance of the R_{sei} and R_{ct} are 306.0, 233.1, 171.0 and 152.6 Ω for M523, MS1, MS3 and MS5, respectively. It is shown that the R_{sei} and R_{ct} of the modified samples are significantly smaller than those of the pristine one. The MS3 and MS5 samples show lower total resistance, which may be relative to the formed Li^+-conductive Li_2SnO_3. This is helpful for the intercalation/de-intercalation of Li ions during the charge/discharge process. To investigate the influence of bulk performance of $LiNi_{0.5}Co_{0.2}Mn_{0.3}O_2$ modified by Sn-doping on electrochemical performance, the relationships between $\omega^{-1/2}$ and Z' based on the experimental results are shown in Figure S2. The apparent Li^+ diffusion coefficient was calculated via a widely used method [8], and it was 1.64×10^{-10}, 1.75×10^{-10} 2.11×10^{-10} and 1.82×10^{-10} cm^2 S^{-1} for M523, MS1, MS3 and MS5, respectively. Hence, it could be claimed that Sn-modification contributes to decreasing the charge transfer impedance and improving the Li^+ diffusion, resulting in better capacity reversibility.

4. Conclusions

Uniform near-spherical Sn-doping and Li_2SnO_3 co-modified $LiNi_{0.5}Co_{0.2}Mn_{0.3}O_2$ were obtained using a facile molten salt method with $0.76LiOH{\cdot}H_2O$-$0.12Li_2CO_3$, commercial $Ni_{0.5}Co_{0.2}Mn_{0.3}(OH)_2$ and Sn nano-powders as the raw materials. The crystal structures, morphologies and electrochemical properties were investigated in detail. The results of the analyses indicate that suitable stannum-modified samples exhibit low cation mixing degrees, enhanced rate capabilities and excellent cyclic performances. Notably, the MS3 sample with 3 mol % Sn-modification aimed at the transition metal site maintained a capacity of 146.8 mAh g^{-1} at the current density of 5C, corresponding to 75.8% of its low rate capacity (0.1C, 193.7mAh g^{-1}), while the pristine one kept the capacity of 116.0 mAh g^{-1}, just 56.9% of its initial capacity (0.1C, 203.9 mAh g^{-1}). The pristine sample also kept the reversible capacity of 157.3 mAh g^{-1} as well as a favorable capacity retention of 88.4% after 100 cycles (2.7–4.6 V, 1C), which is 15.2% higher than that of the pristine M523 (124.9 mAh g^{-1}, 73.2%). The MS3 sample exhibited a lower mole fraction of Ni^{3+}, implying less structural transition during the charge–discharge cycles. The improvement of the electrochemical properties can be attributed to the suitable Sn-substituting and formed Li^+-conductive Li_2SnO_3, which can relieve the cation mixing degree, offer more stable crystalline structure for the fast Li^+-intercalation/de-intercalation during repeated cycles and improve the conductivity to obtain enhanced high-rate reversibility and cycle stability. These results illustrate that Sn-modified $LiNi_{0.5}Co_{0.2}Mn_{0.3}O_2$ is an excellent cathode material for increasingly wide utilization in the fields of electric vehicles and energy storage systems.

Supplementary Materials: The following are available online at http://www.mdpi.com/2079-4991/10/5/868/s1, Figure S1: XPS spectra of the synthesized materials: Co $2p_{3/2}$ (a), Mn $2p_{3/2}$ (c) spectra of M523, Co $2p_{3/2}$ (b), Mn $2p_{3/2}$ (d) spectra of MS3; Figure S2: The relationships between $\omega^{-1/2}$ and Z'.

Author Contributions: Methodology and Conceptualization, H.Z., Y.T., and Z.C.; Resources, S.Z. and J.L.; Formal analysis, H.Z., R.S., X.Y., and Z.F.; Writing—original draft preparation, H.Z.; Writing—review and editing, Z.C.; Funding acquisition, H.Z., L.S., and Z.C. All authors have read and agreed to the published version of the manuscript.

Funding: This research was funded by the National Natural Science Foundation of China (Nos. 51604042, 21501015, 51874048), the Scientific Research Foundation of Hunan Provincial Education Department (Nos. 19B010, 19A003).

Conflicts of Interest: The authors declare no conflict of interest.

References

1. Tarascon, J.-M.; Armand, M. Issues and challenges facing rechargeable lithium batteries. *Nature* **2001**, *414*, 359–367. [CrossRef]
2. Lu, H.; Zhu, Y.; Zheng, B.; Du, H.; Zheng, X.; Liu, C.; Yuan, Y.; Fang, J.; Zhang, K. A hybrid ionic liquid-based electrolyte for high-performance lithium–sulfur batteries. *New J. Chem.* **2020**, *44*, 361–368. [CrossRef]
3. Zheng, J.; Yao, Y.; Mao, G.; Chen, H.; Li, H.; Cao, L.; Ou, X.; Yu, W.; Ding, Z.; Tong, H. Iron–zinc sulfide $Fe_2Zn_3S_5/Fe_{1-x}S$@C derived from a metal–organic framework as a high performance anode material for lithium-ion batteries. *J. Mater. Chem. A* **2019**, *7*, 16479–16487. [CrossRef]
4. Wang, X.; Tan, Y.; Liu, Z.; Fan, Y.; Li, M.; Younus, H.A.; Duan, J.; Deng, H.; Zhang, S. New insight into the confinement effect of microporous carbon in Li/Se battery chemistry: A cathode with enhanced conductivity. *Small* **2020**, 2000266. [CrossRef]
5. Qu, Y.; Guo, M.; Wang, X.; Yuan, C. Novel nitrogen-doped ordered mesoporous carbon as high-performance anode material for sodium-ion batteries. *J. Alloys Compd.* **2019**, *791*, 874–882. [CrossRef]
6. Manthiram, A.; Knight, J.C.; Myung, S.-T.; Oh, S.-M.; Sun, Y.-K. Nickel-rich and lithium-rich layered oxide cathodes: Progress and perspectives. *Adv. Energy Mater.* **2016**, *6*, 1501010. [CrossRef]
7. Chen, Z.; Xu, M.; Du, B.; Zhu, H.; Xie, T.; Wang, W. Morphology control of lithium iron phosphate nanoparticles by soluble starch-assisted hydrothermal synthesis. *J. Power Sources* **2014**, *272*, 837–844. [CrossRef]
8. Liu, Q.; Zhu, H.; Liu, J.; Liao, X.; Tang, Z.; Zhou, C.; Yuan, M.; Duan, J.; Li, L.; Chen, Z. High-performance lithium-rich layered oxide material: Effects of preparation methods on microstructure and electrochemical properties. *Materials* **2020**, *13*, 334. [CrossRef]
9. Liu, J.; Liu, Q.; Zhu, H.; Lin, F.; Ji, Y.; Li, B.; Duan, J.; Li, L.; Chen, Z. Effect of different composition on voltage attenuation of Li-rich cathode material for lithium-ion batteries. *Materials* **2020**, *13*, 40. [CrossRef]
10. Ji, Y.; Zhou, C.; Lin, F.; Li, B.; Yang, F.; Zhu, H.; Duan, J.; Chen, Z. Submicron-sized Nb-doped lithium garnet for high ionic conductivity solid electrolyte and performance of quasi-solid-state lithium battery. *Materials* **2020**, *13*, 560. [CrossRef]
11. Jung, S.-K.; Gwon, H.; Hong, J.; Park, K.-Y.; Seo, D.-H.; Kim, H.; Hyun, J.; Yang, W.; Kang, K. Understanding the degradation mechanisms of $LiNi_{0.5}Co_{0.2}Mn_{0.3}O_2$ cathode material in lithium ion batteries. *Adv. Energy Mater.* **2013**, *4*, 201300787.
12. Su, Y.; Cui, S.; Zhuo, Z.; Yang, W.; Wang, X.; Pan, F. Enhancing the high-voltage cycling performance of $LiNi_{0.5}Co_{0.2}Mn_{0.3}O_2$ by retarding its interfacial reaction with an electrolyte by atomic-layer-deposited Al_2O_3. *ACS Appl. Mater. Interfaces* **2015**, *7*, 25105–25112. [CrossRef] [PubMed]
13. Shi, Y.; Zhang, M.; Qian, D.; Meng, Y.S. Ultrathin Al_2O_3 coatings for improved cycling performance and thermal stability of $LiNi_{0.5}Co_{0.2}Mn_{0.3}O_2$ cathode material. *Electrochim. Acta* **2016**, *203*, 154–161. [CrossRef]
14. Tao, T.; Chen, C.; Qi, W.; Liang, B.; Yao, Y.; Lu, S.-G. Antimony doped tin oxide-coated $LiNi_{0.5}Co_{0.2}Mn_{0.3}O_2$ cathode materials with enhanced electrochemical performance for lithium-ion batteries. *J. Alloys Compd* **2018**, *765*, 601–607. [CrossRef]
15. Liu, K.; Yang, G.-L.; Dong, Y.; Shi, T.; Chen, L. Enhanced cycling stability and rate performance of $Li[Ni_{0.5}Co_{0.2}Mn_{0.3}]O_2$ by CeO_2 coating at high cut-off voltage. *J. Power Sources* **2015**, *281*, 370–377. [CrossRef]
16. Liu, T.; Zhao, S.-X.; Wang, K.; Nan, C.-W. CuO-coated $Li[Ni_{0.5}Co_{0.2}Mn_{0.3}]O_2$ cathode material with improved cycling performance at high rates. *Electrochim. Acta* **2012**, *85*, 605–611. [CrossRef]
17. Yang, J.; Yu, Z.; Yang, B.; Liu, H.; Hao, J.; Yu, T.; Chen, K. Electrochemical characterization of Cr_8O_{21} modified $LiNi_{0.5}Co_{0.2}Mn_{0.3}O_2$ cathode material. *Electrochim. Acta* **2018**, *266*, 342–347. [CrossRef]

18. Wu, F.; Tian, J.; Su, Y.; Guan, Y.; Jin, Y.; Wang, Z.; He, T.; Bao, L.; Chen, S. Lithium-active molybdenum trioxide coated $LiNi_{0.5}Co_{0.2}Mn_{0.3}O_2$ cathode material with enhanced electrochemical properties for lithium-ion batteries. *J. Power Sources* **2014**, *269*, 747–754. [CrossRef]
19. Chen, C.; Tao, T.; Qi, W.; Zeng, H.; Wu, Y.; Liang, B.; Yao, Y.; Lu, S.; Chen, Y. High-performance lithium ion batteries using SiO_2-coated $LiNi_{0.5}Co_{0.2}Mn_{0.3}O_2$ microspheres as cathodes. *J. Alloys Compd.* **2017**, *709*, 708–716. [CrossRef]
20. Liu, W.; Wang, M.; Gao, X.; Zhang, W.; Chen, J.; Zhou, H.; Zhang, X. Improvement of the high-temperature, high-voltage cycling performance of $LiNi_{0.5}Co_{0.2}Mn_{0.3}O_2$ cathode with TiO_2 coating. *J. Alloys Compd.* **2012**, *543*, 181–188. [CrossRef]
21. Kong, J.-Z.; Ren, C.; Tai, G.-A.; Zhang, X.; Li, A.-D.; Wu, D.; Li, H.; Zhou, F. Ultrathin ZnO coating for improved electrochemical performance of $LiNi_{0.5}Co_{0.2}Mn_{0.3}O_2$ cathode material. *J. Power Sources* **2014**, *266*, 433–439. [CrossRef]
22. Schipper, F.; Bouzaglo, H.; Dixit, M.; Erickson, E.M.; Weigel, T.; Talianker, M.; Grinblat, J.; Burstein, L.; Schmidt, M.; Lampert, J.; et al. From Surface ZrO_2 coating to bulk Zr doping by high temperature annealing of nickel-rich lithiated oxides and their enhanced electrochemical performance in lithium ion batteries. *Adv. Energy Mater.* **2018**, *8*, 1701682. [CrossRef]
23. Yang, K.; Fan, L.-Z.; Guo, J.; Qu, X. Significant improvement of electrochemical properties of AlF_3-coated $LiNi_{0.5}Co_{0.2}Mn_{0.3}O_2$ cathode materials. *Electrochim. Acta* **2012**, *63*, 363–368. [CrossRef]
24. Li, L.; Zhang, Z.; Fu, S.; Liu, Z.; Liu, Y. Co-modification by $LiAlO_2$-coating and Al-doping for $LiNi_{0.5}Co_{0.2}Mn_{0.3}O_2$ as a high-performance cathode material for lithium-ion batteries with a high cutoff voltage. *J. Alloys Compd* **2018**, *768*, 582–590. [CrossRef]
25. Hu, W.; Zhang, C.; Jiang, H.; Zheng, M.; Wu, Q.-H.; Dong, Q. Improving the electrochemistry performance of layer $LiNi_{0.5}Co_{0.2}Mn_{0.3}O_2$ material at 4.5 V cutoff potential using lithium metaborate. *Electrochim. Acta* **2017**, *243*, 105–111. [CrossRef]
26. Yang, X.; Wang, X.; Hu, L.; Zou, G.; Su, S.; Bai, Y.; Shu, H.; Wei, Q.; Hu, B.; Ge, L.; et al. Layered $Li[Ni_{0.5}Co_{0.2}Mn_{0.3}]O_2$–$Li_2MnO_3$ core–shell structured cathode material with excellent stability. *J. Power Sources* **2013**, *242*, 589–596. [CrossRef]
27. Zhang, M.; Hu, G.; Liang, L.; Peng, Z.; Du, K.; Cao, Y. Improved cycling performance of Li_2MoO_4-inlaid $LiNi_{0.5}Co_{0.2}Mn_{0.3}O_2$ cathode materials for lithium-ion battery under high cutoff voltage. *J. Alloys Compd.* **2016**, *673*, 237–248. [CrossRef]
28. Hu, G.; Zhang, M.; Wu, L.; Peng, Z.; Du, K.; Cao, Y. Effects of Li_2SiO_3 coating on the performance of $LiNi_{0.5}Co_{0.2}Mn_{0.3}O_2$ cathode material for lithium ion batteries. *J. Alloys Compd.* **2017**, *690*, 589–597. [CrossRef]
29. Wang, J.; Yu, Y.; Li, B.; Fu, T.; Xie, D.; Cai, J.; Zhao, J. Improving the electrochemical properties of $LiNi_{0.5}Co_{0.2}Mn_{0.3}O_2$ at 4.6 V cutoff potential by surface coating with Li_2TiO_3 for lithium-ion batteries. *Phys. Chem. Chem. Phys.* **2015**, *17*, 32033–32043. [CrossRef]
30. Huang, Y.; Jin, F.-M.; Chen, F.-J.; Chen, L. Improved cycle stability and high-rate capability of Li_3VO_4-coated $Li[Ni_{0.5}Co_{0.2}Mn_{0.3}]O_2$ cathode material under different voltages. *J. Power Sources* **2014**, *256*, 1–7. [CrossRef]
31. Xu, Y.; Liu, Y.; Lu, Z.; Wang, H.; Sun, D.; Yang, G. The preparation and role of Li_2ZrO_3 surface coating $LiNi_{0.5}Co_{0.2}Mn_{0.3}O_2$ as cathode for lithium-ion batteries. *App. Surf. Sci.* **2016**, *361*, 150–156. [CrossRef]
32. Song, H.; Yuan, H.; Chen, H.; Tang, A.; Xu, G.; Liu, L.; Zhang, Z.; Kuang, Q. Synthesis of TiO_2/S@PPy composite for chemisorption of polysulfides in high performance Li-S batteries. *J. Solid State Electr.* **2020**. [CrossRef]
33. Wu, Z.; Han, X.; Zheng, J.; Wei, Y.; Qiao, R.; Shen, F.; Dai, J.; Hu, L.; Xu, K.; Lin, Y.; et al. Depolarized and fully active cathode based on $Li(Ni_{0.5}Co_{0.2}Mn_{0.3})O_2$ embedded in carbon nanotube network for advanced batteries. *Nano Lett.* **2014**, *14*, 4700–4706. [CrossRef] [PubMed]
34. Li, G.; Zhang, Z.; Wang, R.; Huang, Z.; Zuo, Z.; Zhou, H. Effect of trace Al surface doping on the structure, surface chemistry and low temperature performance of $LiNi_{0.5}Co_{0.2}Mn_{0.3}O_2$ cathode. *Electrochim. Acta* **2016**, *212*, 399–407. [CrossRef]
35. Dixit, M.; Markovsky, B.; Aurbach, D.; Major, D.T. Unraveling the effects of Al doping on the electrochemical properties of $LiNi_{0.5}Co_{0.2}Mn_{0.3}O_2$ using first principles. *J. Electrochem. Soc.* **2017**, *164*, A6359–A6365. [CrossRef]

36. Chen, Z.; Gong, X.; Zhu, H.; Cao, K.; Liu, Q.; Liu, J.; Li, L.; Duan, J. High performance and structural stability of K and Cl co-doped $LiNi_{0.5}Co_{0.2}Mn_{0.3}O_2$ cathode materials in 4.6 voltage. *Front. Chem.* **2018**, *6*, 643. [CrossRef]
37. Li, Y.; Su, Q.; Han, Q.; Li, P.; Li, L.; Xu, C.; Cao, X.; Cao, G. Synthesis and characterization of Mo-doped $LiNi_{0.5}Co_{0.2}Mn_{0.3}O_2$ cathode materials prepared by a hydrothermal process. *Ceram. Int.* **2017**, *43*, 3483–3488. [CrossRef]
38. Hua, W.; Zhang, J.; Zheng, Z.; Liu, W.; Peng, X.; Guo, X.D.; Zhong, B.; Wang, Y.J.; Wang, X. Na-doped Ni-rich $LiNi_{0.5}Co_{0.2}Mn_{0.3}O_2$ cathode material with both high rate capability and high tap density for lithium ion batteries. *Dalton Trans.* **2014**, *43*, 14824–14832. [CrossRef]
39. Zhao, R.; Yang, Z.; Liang, J.; Lu, D.; Liang, C.; Guan, X.; Gao, A.; Chen, H. Understanding the role of Na-doping on Ni-rich layered oxide $LiNi_{0.5}Co_{0.2}Mn_{0.3}O_2$. *J. Alloys Compd.* **2016**, *689*, 318–325. [CrossRef]
40. Mo, Y.; Guo, L.; Cao, B.; Wang, Y.; Zhang, L.; Jia, X.; Chen, Y. Correlating structural changes of the improved cyclability upon Nd-substitution in $LiNi_{0.5}Co_{0.2}Mn_{0.3}O_2$ cathode materials. *Energy Storage Mater.* **2019**, *18*, 260–268. [CrossRef]
41. Zhang, Y.; Wang, Z.-B.; Lei, J.; Li, F.-F.; Wu, J.; Zhang, X.-G.; Yu, F.-D.; Ke, K. Investigation on performance of $Li(Ni_{0.5}Co_{0.2}Mn_{0.3})_{1-x}Ti_xO2$ cathode materials for lithium-ion battery. *Ceram. Int.* **2015**, *41*, 9069–9077. [CrossRef]
42. Chen, Y.; Li, Y.; Li, W.; Cao, G.; Tang, S.; Su, Q.; Deng, S.; Guo, J. High-voltage electrochemical performance of $LiNi_{0.5}Co_{0.2}Mn_{0.3}O_2$ cathode material via the synergetic modification of the Zr/Ti elements. *Electrochim. Acta* **2018**, *281*, 48–59. [CrossRef]
43. Zhao, X.; Liang, G.; Liu, H.; Liu, Y. Improved conductivity and electrochemical properties of $LiNi_{0.5}Co_{0.2}Mn_{0.3}O_2$ materials via yttrium doping. *RSC Adv.* **2018**, *8*, 4142–4152. [CrossRef]
44. Wang, D.; Wang, Z.; Li, X.; Guo, H.; Xu, Y.; Fan, Y.; Pan, W. Effect of surface fluorine substitution on high voltage electrochemical performances of layered LiNi0.5Co0.2Mn0.3O2 cathode materials. *Appl. Surf. Sci.* **2016**, *371*, 172–179. [CrossRef]
45. Zhang, Y.; Wang, Z.-B.; Yu, F.-D.; Que, L.-F.; Wang, M.-J.; Xia, Y.-F.; Xue, Y.; Wu, J. Studies on stability and capacity for long-life cycle performance of $Li(Ni_{0.5}Co_{0.2}Mn_{0.3})O_2$ by Mo modification for lithium-ion battery. *J. Power Sources* **2017**, *358*, 1–12. [CrossRef]
46. Qiao, Q.; Qin, L.; Li, G.; Wang, Y.; Gao, X. Sn-stabilized Li-rich layered $Li(Li_{0.17}Ni_{0.25}Mn_{0.58})O_2$ oxide as a cathode for advanced lithium-ion batteries. *J. Mater. Chem. A* **2015**, *3*, 17627–17634. [CrossRef]
47. Li, J.; He, X.; Zhao, R.; Wan, C.; Jiang, C.; Xia, D.; Zhang, S. Stannum doping of layered $LiNi_{3/8}Co_{2/8}Mn_{3/8}O_2$ cathode materials with high rate capability for Li-ion batteries. *J. Power Sources* **2006**, *158*, 524–528. [CrossRef]
48. Ma, X.; Wang, C.; Cheng, J.; Sun, J. Effects of Sn doping on the structural and electrochemical properties of $LiNi_{0.8}Co_{0.2}O_2$ cathode materials. *Solid State Ion.* **2007**, *178*, 125–129. [CrossRef]
49. Song, L.; Li, A.; Xiao, Z.; Chi, Z.; Cao, Z.; Zhu, H. Enhanced electrochemical properties of Ni-rich $LiNi_{0.8}Co_{0.1}Mn_{0.1}O_2$ by SnO_2 coating under high cutoff voltage. *Ionics* **2020**. [CrossRef]
50. Liu, X.; Kou, L.; Shi, T.; Liu, K.; Chen, L. Excellent high rate capability and high voltage cycling stability of Y_2O_3-coated $LiNi_{0.5}Co_{0.2}Mn_{0.3}O_2$. *J. Power Sources* **2014**, *267*, 874–880. [CrossRef]